Novel X-ray multi-spectral imaging of ultraintense laser plasmas by a single-photon CCD based pinhole camera

L. Labate,* A. Giulietti,* D. Giulietti,† P. Köster,† T. Levato,† and L.A. Gizzi*
Intense Laser Irradiation Laboratory - IPCF, Consiglio Nazionale delle Ricerche, Via Moruzzi 1, 56124 Pisa, Italy
e-mail: luca.labate@ipcf.cnr.it; URL: http://ilil.ipcf.cnr.it

F. Zamponi, A. Lübcke, T. Kämpfer, I. Uschmann, and E. Förster
Institut für Optik und Quantenelektronik - Friedrich-Schiller-Universität, Max-Wien-Platz 1, 07743 Jena, Germany

Spectrally resolved two-dimensional imaging of ultrashort laser-produced plasmas is described, obtained by means of an advanced technique. The technique has been tested with microplasmas produced by ultrashort relativistic laser pulses. The technique is based upon the use of a pinhole camera equipped with a CCD detector operating in the single-photon regime. The spectral resolution is about 150 eV in the $4-10$ keV range and images in any selected photon energy range have a spatial resolution of $5\,\mu$m. The potential of the technique to study fast electron propagation in ultraintense laser interaction with multilayer targets is discussed and some preliminary results are shown.

PACS numbers:

I. INTRODUCTION

Plasmas produced by ultrashort and ultraintense laser pulses are currently investigated for their importance both as ultrashort, monochromatic X-ray sources [1, 2] and as sources of fast electrons in the fast ignitor scheme for Inertial Confinement Fusion (ICF) [3, 4]. The basic process responsible for the K-shell emission in such plasmas is the generation and the subsequent propagation of fast electrons inside the cold or partially ionized target material. As a consequence, Kα emission is a fundamental diagnostics for these electrons [5–9]. Furthermore, the Bremsstrahlung emission, occurring in the X-ray range, from the fast electrons has an important role, from both a theoretical and an experimental viewpoint [10, 11].
Bent Bragg crystals coupled either to X-ray films or to CCD detectors are among the most commonly used X-ray diagnostics for the laser-plasma X-ray emission. Spectral resolutions down to a few eV and a simultaneous 1D spatial resolution of some microns can be reached in this way [6, 12–14]. Simultaneous monochromatic X-ray images of an ICF target at different X-ray energies in a narrow range from about 3500 to 4100 eV have been recently obtained using a flat Bragg crystal and a pinhole array [15]. Scintillation photomultiplier detectors coupled to K-edge filters for spectral selection [16] or cooled Ge detectors in single-photon counting mode [17] have also been used for high energy X-ray spectroscopy of laser plasmas, with no spatial resolution.
While allowing spatial resolution to be achieved, bent crystals in the Bragg configuration suffer from some drawbacks. For instance, due to the narrow rocking curve, usually much smaller than the width of the spectral line of interest, the efficiency can be quite low [18]. Furthermore, the reflectivity generally decreases at high photon energies. Concerning the spatial resolution, the small Bragg angles usually needed at high photon energies lead to strong image aberrations [19]. Another important drawback of bent crystals arises from their efficient reflectivity extending, in some cases, over many diffraction orders [12], which results in an overlapping of the contributions from different orders on the same image. Finally, crystals can produce fluorescence and Compton radiation when exposed to hard X-rays, as well as X-ray radiation due to the interaction with high energy particles. This can significantly contribute to the background noise on the detector, in particular in relativistic laser-plasma interaction environments [20].
For such reasons, the use of CCD detectors in the so-called single-photon regime for ultrashort and ultraintense laser-plasma X-ray spectroscopy is now being considered [21, 22], in particular in sub-PW or PW laser interaction regimes [23]. As it is well known, CCD detectors, while still limited in spatial resolution when compared to X-ray films, offer a number of advantages such as high linearity, dynamic range and quantum efficiency, as well as a much faster visualization of the data and digital image processing [24, 25]. When used in the single-photon regime, a CCD detector enables the spectrum of the impinging X-ray radiation to be obtained without any additional dispersive device. This is basically due to the fact that each X-ray photon absorbed in the sensitive layer of the CCD gives rise to a signal (charge) proportional to the photon energy [26, 27]. Due to the large number of pixels in a conventional CCD chip, a few laser shots (ideally one) are required to get an X-ray spectrum in a large energy interval, with a typical resolution which, in the energy range from 1 keV up to a few tens of keV (see, e.g. [28, 29] and References therein), can be well below 10%.

*Also at INFN, Sezione di Pisa, Italy
†Also at Dipartimento di Fisica, Università di Pisa and INFN, Sezione di Pisa, Italy

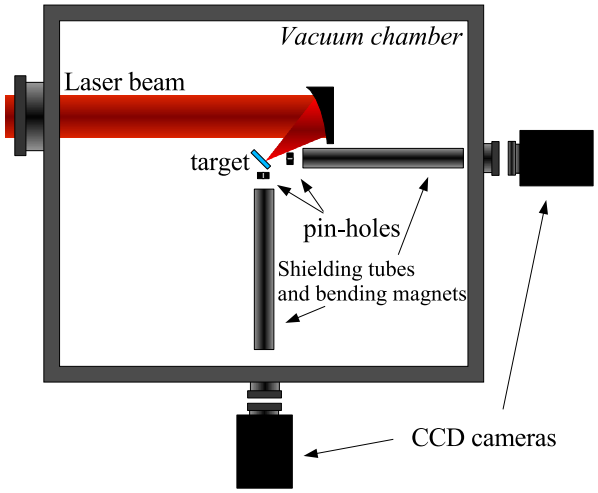

FIG. 1: Layout of the experimental setup.

Early attempts of using CCD detectors in single-photon regime for multi-spectral imaging date back to Eighties [30, 31]. Recently, noteworthy experimental results were obtained in the field of multi-spectral radiography and projection microscopy, using CCDs or other solid-state area detectors [32, 33].

In this paper we report on the test of a different, advanced technique which, while relying on such a CCD detector operating in a single-photon regime, employs a pinhole to get spectrally resolved, two-dimensional images (or, in other words, X-ray spectra with 2D spatial resolution) of a micrometer-size laser-produced plasma. A similar technique have recently been used for an Electron Cyclotron Resonance plasma [34, 35]. In such a case, an ECR plasma chamber of a few centimeters was imaged out, using a 70 μm pinhole, with a spatial resolution of about 0.1 mm. Exposure times from a few up to some hundreds of milliseconds were used and a number of more than 500 exposures was tipically needed. In our case a micrometer-size plasma produced by ultrashort, relativistic laser pulse irradiation of solid targets was successfully imaged out with a spectral resolution down to about 150 eV and a spatial resolution of some microns. To our knowledge, this is the first report of the use of such a technique as a diagnostics of a laser-produced plasma. A description of the test experimental setup is reported in Section II, followed by a discussion of the main aspects of the technique, including the data analysis, in Section III. The preliminary results of this technique applied to the study of the electron propagation in multilayer targets are then reported in Section IV.

II. THE TEST EXPERIMENTAL SETUP

A schematic layout of the experimental setup is shown in Figure (figure1). The 8 TW Ti:Sa laser system at IOQ-Jena has been used to irradiate thin foil targets at relativistic intensities. The laser provides 70 fs duration pulses with 600 mJ energy at a 10 Hz repetition rate. A 45 deg, $f/1.2$ off-axis parabola has been used to focus the laser beam onto the target surface down to a 5 μm^2 spot, thus reaching an intensity of about 5×10^{19} W/cm^2 (normalized vector potential $a_0 = eA_L/m_e c^2 \simeq 4.8$). The angle of incidence on the target was about 10 deg. The target was moved horizontally or vertically to ensure a fresh surface to be irradiated at each shot.

The target consisted of a sandwich of layers of different Z materials. These targets were designed to study the fast electron propagation inside the target by detecting the $K\alpha$ emission from each layer.

Two pinhole cameras were used to image out the X-ray emission from both the front and rear side of the target. The viewing angle was about 45 deg with respect to the surface. As it will be examined carefully below, energy resolution was also obtained by these diagnostics, on a multi-shot basis, by letting them operate in the so-called single-photon regime. Each pinhole camera consisted of a 5 μm diameter pinhole, bored in a 25 μm thick Pt substrate, and a back-illuminated, deep depletion Andor DX420 CCD camera, whose response and QE were previously studied using a Si diode [36] (as reported in this latter paper, QE varies from about 90 to 60 percent in the energy range considered here). The 1024x256 pixel CCD chip (Andor DX420) was tipically cooled at $-65\,^{\circ}$C.

The two pinholes were put about 30 mm away from the target, on both the front and rear side, and were protected from debris by using a 600 nm thick *mylar* foil. In order to obtain the required magnification, $M \simeq 10$, the two CCD cameras were placed outside the main vacuum chamber, in separate vacuum chambers equipped with 50 μm thick *kapton* windows (about 96% transmission at 4.5 keV). An additional Be filter was used to shield CCDs against visible light.

As it can be seen in the Figure, a lead tube was set up, with walls about 10 mm thick and a clear aperture of about 10 mm diameter, along each pinhole camera main axis. These tubes allowed us to shield the CCD detectors against X-ray photons scattered inside the vacuum chamber. Also, a set of magnets (with typical magnetic field strength of about 0.3 T) were placed inside each tube in order to stop high-energy electrons. Indeed, as it is well known (see e.g. the papers cited in the Introduction), electrons with typical energy as high as some MeV can be expected to be produced in our experimental conditions. Multiple pairs of such magnets were employed to deviate these electrons, almost filling the lead tubes shown in the Figure along their whole length.

Given the pinhole camera magnification (10x) and considering the pixel size of the two CCDs (26×26 μm^2), the

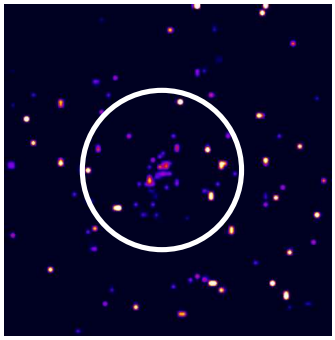

FIG. 2: Typical raw image as provided by our detectors. Such an image is obtained from one laser shot.

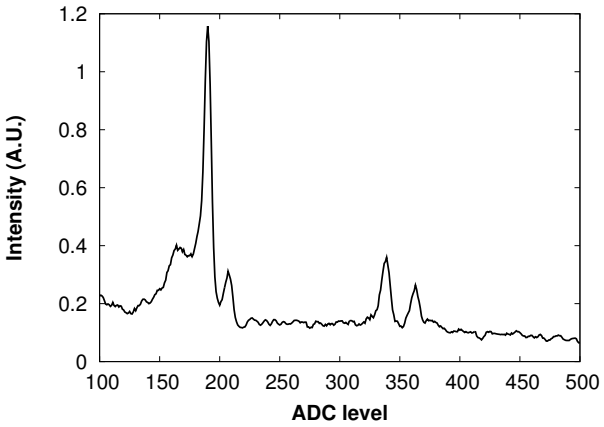

FIG. 3: Pulse height distribution obtained from 350 laser shots irradiation of a Ti-Cu target, for the front side diagnostics shown in Figure (figure1).

spatial resolution achievable by the pinhole cameras was mainly limited by the pinhole size and is expected to be approximately 5 μm in the object plane. With this value of the magnification, a typical ultrashort laser-plasma X-ray source having sizes of about 30 μm, as in our case, would involve roughly a 15x15 pixel wide region of the chip. Due to the single-photon condition to be satisfied, this led to an average number of the order of about 30 photons to be detected per acquisition.
Finally, in order for the two CCD cameras to operate in the single-photon regime, up to 20 mylar foils (each one 50 μm thick) were used for each pinhole camera to reduce the flux to the required level. Due to the different photon flux, the number of foils used was in general different for the two CCDs.

III. DESCRIPTION OF THE TECHNIQUE

As it was said in Section I, in principle, a CCD detector enables the X-ray spectrum of a given source to be retrieved without any external dispersive device, provided that an average of no more than one photon hits each pixel (in practice, due to the charge spreading around neighbouring pixels, this number must be less than one [37]). In our case this feature was exploited by forcing the CCD detectors to operate in the single-photon condition. As it was said above, this was accomplished by reducing the X-ray flux per laser shot by means of mylar filters. Figure (figure2) shows, as an example, a typical image obtained from the front-side pinhole camera, consisting of a collection of spots (each with its own shape and signal amplitude) corresponding to single photon interactions with the CCD detector. The greater concentration of such spots occurs near the center of the shown area, corresponding to the center of the image of the X-ray source as provided by the pinhole. Each CCD acquisition (corresponding to one laser shot) was then analyzed in order to retrieve the total released charge and the landing position on the chip surface of each X-ray photon. In fact, a number of physical processes occur in the CCD structure demanding for a careful analysis [26, 38]. These processes can give rise either to a spreading of the charge cloud produced by the impinging photons [39, 40] or to a loss of a fraction of this charge [41]. For such a reason, a dedicated reconstruction algorithm has been used in our case, based upon previous works [36, 42]. As a result, the spectrum of the X-ray emission from the target has been obtained, after summing up the contribution from a few hundreds laser shots (i.e., CCD acquisitions).

As an example, Figure (figure3) shows the pulse height distribution for the front side CCD, as obtained by adding photons from 350 laser shots on a Ti-mylar-Cu target. The X-ray spectrum can be obtained from this pulse height distribution once the CCD response is known. The peaks corresponding to the Kα ($\sim$ 4.5 keV) and Kβ ($\sim$ 4.9 keV) lines from Ti are visible, at about 180 ADC levels, as well as to the Kα ($\sim$ 8 keV) and Kβ ($\sim$ 8.9 keV) emission lines from Cu at about 350 ADC levels.

The full image of the source, integrated over the whole spectrum, can be directly obtained by summing up the signal from a given set of CCD acquisitions. On the other hand, an image of the source in a selected photon energy range can be obtained by selecting only photons in that range. Figure (figure4) *left* shows the image of the X-ray source, as seen by the front-side pinhole camera, at the Ti Kα and Kβ energy (that is, taking into account photons at both the Kα and Kβ energy), obtained from the same set of shots of Figure (figure3). As discussed in the previous Section, the spatial resolution of such an image due to the imaging system can be estimated to be about 5 μm. However, due to the multi-shot integration, some image resolution degradation may occur as a consequence of source displacement due to laser beam pointing instability, target surface imperfections, etc. These effects have been partially reduced, in our analysis, by considering the photon position relative to an average origin point, different from shot to shot. In other words, for each ac-

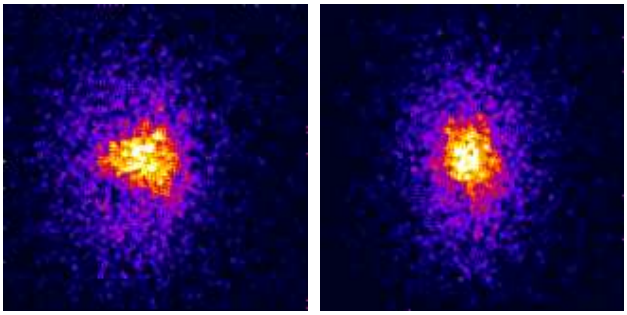

FIG. 4: *left:* Image of the X-ray source at the Ti Kα and Kβ energy (that is, considering together photons at both the Kα and Kβ energy of Ti) as seen from the front side of the target. The image refers to the same set of shots of Figure (figure3) (350 shots on a Ti-mylar-Cu target). The image size is 200 μm (in the object plane) in both the horizontal and vertical direction. *right:* Same as at left, but after the correction for the target position changes from shot to shot.

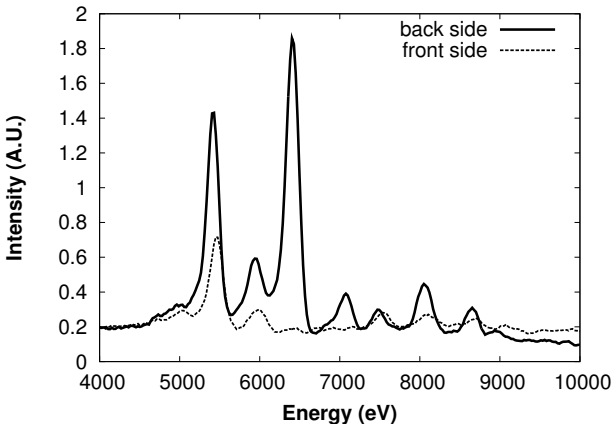

FIG. 5: X-ray spectrum obtained from 350 laser shots irradiation of a Cr-Ni-Fe target.

quisition, the position on the detector surface of the point defined by $(\bar{x}_i, \bar{y}_i) = \sum_j (x_j^{(i)}, y_j^{(i)})/N_{ph}^{(i)}$ (where the index i identifies the acquisition, $x_j^{(i)}$ and $y_j^{(i)}$ are the coordinates of the j-th photon of the acquisition i and $N_{ph}^{(i)}$ is the total number of photons in the acquisition) has been calculated as a first step. Data from different shots have then be summed up as relative to a common origin given for each shot by the position of this point. Since the error on the coordinates $(\bar{x}_i, \bar{y}_i)$ depends upon the number of photons detected in each acquisition, only acquisitions (namely, shots) with this number above a threshold value (that is, with a minimum number of photons) has been considered. We observe that such an approach, in general, is not valid as it may lead to artifacts or image deformation. Post-facto considerations, along with additional information concerning the specific experimental set-up may help in assessing the reliability of this image correction. In particular, in our case, the values of $(\bar{x}_i, \bar{y}_i)$ showed a well defined, regular correlation with the shot number i (laser focal spot position on target), which we easily were able to attribute to residual small imperfections in the target surface (alignment), leading to a small shifts of the X-ray source. The value given above for the spatial resolution in our images takes into account this analysis procedure. As an example, Figure (figure4) *right* shows the improvement resulting from such a correction algorithm. The difference between the two images clearly highlights the shift suffered by our source horizontal position from shot to shot.

IV. APPLICATION TO THE IMAGING OF MULTILAYER TARGETS AND DISCUSSION

As anticipated above, K-shell emission from ultrashort, relativistic laser plasmas can be fruitfully used as a diagnostics for fast electron propagation. In this case, multilayer targets are usually employed in order to distinguish the X-ray emission at different depths inside the target by the "tracer layers" (see [43] and References therein). In this Section we briefly show some results obtained on a 3 metallic layer target, whose K-shell line emission were all detected and imaged. Only those aspects related to the technique will be dealt with, leaving to further papers a discussion of the physical issues.

The target used consisted of a Cr 1.2 μm thick layer (on the front side), a middle layer of Ni, 11 μm thick, and a third layer (on the back side) of Fe of thickness 10 μm.

Figure (figure5) shows the spectrum obtained by our front and back side diagnostics (again, integrated over 350 shots). According to the width of the background ADC level distribution, the spectral resolution in this plot can be estimated to be of about 150 eV. For the sake of interpretation, Table I reports the energies of the Kα and Kβ emission lines from the target materials. As it clearly appears from the difference between the front and back side spectra, the line intensities are strongly affected by the photon propagation through the different layers.

Figure (figure6) shows the images of the X-ray source at the Kα and Kβ line energy of the three materials, as seen by the front and back side diagnostics. As an example, Figure (figure7) shows the horizontal lineout of the emission at the Cr Kα /Kβ energy from the two sides. The images of Figure (figure6) clearly shows some differences in the spatial structure of the source at a fixed energy when viewed from the front and from the back side of the target.

A quantitative comparison of these images would require reabsorption effects to be taken into account. Also, the possible different contribution of the Bremsstrahlung photons to the two images should be considered. These issues will be discussed elsewhere. Here we only point out that our technique is able to resolve the X-ray emission

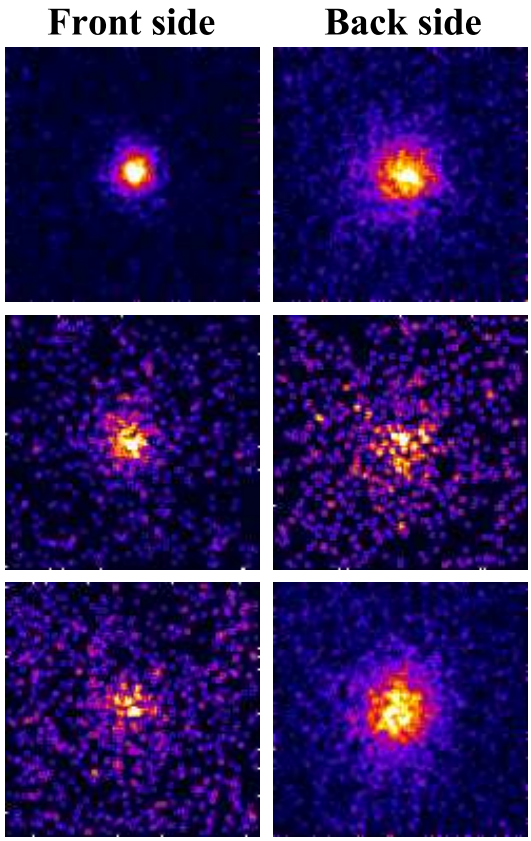

FIG. 6: X-ray images of the source at the Kα and Kβ energy (considered together) of the different target materials, obtained from 350 shots on a Cr-Ni-Fe target: *top:* Cr, *middle:* Ni, *bottom:* Fe. The image size is 156 μm (in the object plane) in both the horizontal and vertical direction.

from the different layers. Also, the images have sufficient spatial resolution to provide valuable informations on the dynamic of fast electron transport of energy in tracer layers. This is the key information required to model experimental observations using dedicated numerical tools.

V. SUMMARY AND CONCLUSIONS

In summary, the 2D imaging with spectral resolution of the X-ray emission from ultrashort laser irradiated targets by using an advanced technique has been reported. The experimental setup is that of a simple pinhole camera, but the CCD detector is forced to operate in the so-called single-photon regime. This regime of operation allows the spectrum of the incoming radiation to be retrieved, provided tha X-ray response of the CCD has been previously characterized. By summing up the contributions from a sufficient number of acquisitions, the image of the X-ray emitting region at the different photon energies can be recovered. Furthermore, the absolute photon

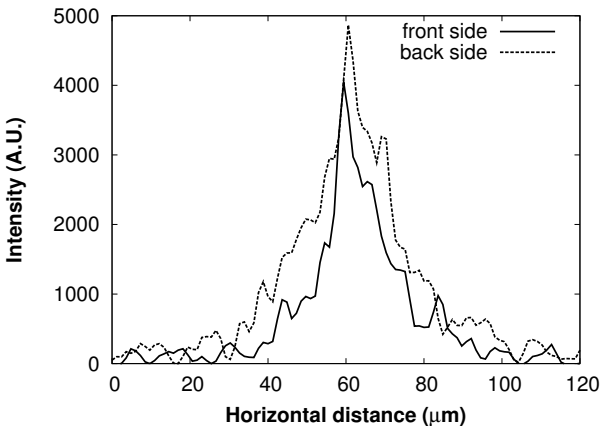

FIG. 7: Lineout along the horizontal direction, integrated over 10 μm in the vertical direction, of the top images of Figure (figure6).

flux in each selected energy range can be retrieved, once the collection efficiency of the setup and the detector QE are considered.

We have shown a first use of the technique for studying the propagation of fast electrons inside the target by using multilayer targets, whose K-shell emission from each layer due to the impact of electrons was successfully imaged with a spatial reolution of about 5 μm and a spectral resolution of about 150 eV. The X-ray emission at a given energy due to Bremsstrahlung radiation can also be imaged in this way.

The technique 'as it is' has currently a 'multi-shot' basis (about 350 laser shots were required in our case), due to the need for a statistically significant number of photons to be detected. This means that it is suitable only for high-repetition rate laser sources. The number of shots could be reduced by using a higher magnification, which would enable to collect a greater number of photons per shot, while satisfying the single-photon condition on the CCD detector. Another possibility is to exploit large area CCDs or similar position sensitive devices in combination with a pinhole array, to collect more than one 'single-photon image' on the same CCD detector. Both the solutions are currently being investigated.

VI. ACKNOWLEDGEMENTS

Access to the Jena facility was granted by the LASERLAB initiative of the 6th Framework Programme of the European Union. The Pisa authors wish to acknowledge support from the Italian MIUR projects FISR "Impianti innovativi multiscopo per la produzione di radiazione X ed ultravioletta", FIRB "BLISS - Broadband Laser for ICF Strategic Studies" and "SPARX". The Pisa group also acknowledge support from the INFN project "PLASMONX - Plasma Acceleration and Monochro-

matic X-ray generation".

[1] A. Rousse, C. Rischel, J.-C. Gauthier, *Rev. Mod. Phys.* **73**, 17-31 (2001)

[2] C. Reich, I. Uschmann, F. Ewald, S. Düsterer, A. Lübcke, H. Schwoerer, R. Sauerbrey, E. Förster, *Phys. Rev. E* **68**, 056408 (2003)

[3] M. Tabak, J. Hammer, M. E. Glinsky, W. L. Kruer, S. C. Wilks, J. Woodworth, E. M. Campbell, M. D. Perry, R. J. Mason, *Phys. Plasmas* **1**, 1626-1634 (1994)

[4] S. Atzeni, *Phys. Plasmas* **6**, 3316-3326 (1999)

[5] P. Gibbon, E. Förster, *Plasma Phys. Controll. Fusion* **38**, 769-793 (1996)

[6] H. Nishimura, T. Kawamura, R. Matsui, Y. Ochi, S. Okihara, S. Sakabe, F. Koike, T. Johzaki, H. Nagatomo, K. Mima, I. Uschmann, E. Förster, *J. Quantum Spectr. Radiat. Transf.* **81**, 327-337 (2003)

[7] R. Freeman, C. Anderson, J. M. Hill, J. King, R. Snavely, S. Hatchett, M. Key, J. Koch, A. MacKinnon, R. Stephens, T. Cowan, *J. Quantum Spectr. Radiat. Transf.* **81**, 183-190 (2003)

[8] D. Batani, A. Antonicci, F. Pisani, T. A. Hall, D. Scott, F. Amiranoff, M. Koenig, L. Gremillet, S. Baton, E. Martinolli, C. Rousseaux, W. Nazarov, *Phys. Rev. E* **65**, 066409 (2002)

[9] K. Yasuike, M. H. Key, S. P. Hatchett, R. A. Snavely, K. B. Wharton, *Rev. Sci. Instrum.* **72**, 1236-1240 (2001)

[10] P. A. Norreys, M. Santala, E. Clark, M. Zepf, F. Watts, F. N. Beg, K. Krushelnick, M. Tatarakis, A. E. Dangor, X. Fang, P. Graham, T. McCanny, R. P. Singhal, K. W.D. Ledingham, A. Creswell, D. C. W. Sanderson, J. Magill, A. Machacek, J. Wark, R. Allott, B. kennedy, D. Neely, *Phys. Plasmas* **6**, 2150-2156 (1999)

[11] Y. Sentoku, K. Mima, T. Taguchi, S. Miyamoto, Y. Kishimoto, *Phys. Plasmas* **5**, 4366-4372 (1998)

[12] G. Hölzer, O. Werhan, J. Heinish, E. Förster, T. A. Pikuz, A. Ya. Faenov, S. A. Pikuz, V. M. Romanova, T. A. Shelkovenko, *Physica Scripta* **57**, 301-309 (1998)

[13] B. K. F. Young, A. L. Osterheld, D. F. Price, R. Shepherd, R. E. Stewart, A. Ya. Faenov, A. I. Magunov, T. A. Pikuz. I. Yu. Skobelev, F. Flora, S. Bollanti, P. Di Lazzaro, T. Letardi, A. Grilli, L. Palladino, A. Reale, A. Scafati, L. Reale, *Rev. Sci. Instrum.* **69**, 4049-4053 (1998)

[14] J. A. King, K. Akli, R. A. Snavely, B. Zhang, M. H. Key, C. D. Chen, S. P. Hatchett, J. A. Koch, A. J. MacKinnon, P. K. Patel, T. Phillips, R. P. J. Town, R. R. Freeman, M. Borghesi, L. Romagnani, M. Zepf, T. Cowan, R. Stephens, K. L. Lancaster, C. D. Murphy, P. Norreys, C. Stoeckl, *Rev. Sci. Instrum.* **76**, 076102 (2005)

[15] R. Tommasini, J. A. Koch, N. Izumi, L. A. Welser, R. C. Mancini, J. Delettrez, S. Regan, V. Smalyuk, *Rev. Sci. Instrum.* **77**, 10E303 (2006)

[16] J. Yu, Z. Jang, J. C. Kieffer, A. Krol, *Phys. Plasmas* **6**, 1318-1322 (1999)

[17] C. Tillmann, S. A. Johansson, B. Erlandsson, M. Grätz, B. Hemdal, A. Almèn, S. Mattsson, S. Svanberg, *Nucl. Instrum. Meth. A* **394**, 387-396 (1997)

[18] T. Missalla, I. Uschmann, E. Förster, G. Jenke, D. von der Linde, *Rev. Sci. Instrum.* **70**, 1288-1299 (1999)

[19] M. Dirksmöller, O. Rancu, I. Uschmann, P. Renaudin, C. Chenais-Popovis, J. C. Gauthier, E. Förster, *Optics Commun.* **118**, 379-387 (1995)

[20] C. Stoeckl, W. Theobald, T. C. Sangster, M. H. Key, P. Patel, B. B. Zhang, R. Clarke, S. Karsch, P. Norreys, *Rev. Sci. Instrum.* **75**, 3705-3707 (2004)

[21] L. A. Gizzi, A. Giulietti, D. Giulietti, P. Audebert, S. Bastiani, J.-P. Geindre, A. Mysyrowicz, *Phys. Rev. Lett.* **76**, 2278-2281 (1996)

[22] L. Labate, M. Galimberti, A. Giulietti, D. Giulietti, P. Köster, P. Tomassini, L. A. Gizzi, *Appl. Phys. B* **86**, 229-233 (2007)

[23] H. S. Park, N. Izumi, M. H. Key, J. A. Koch, O. L. Landen, P. K. Patel, T. W. Phillips, B. B. Zhang, *Rev. Sci. Instrum.* **75**, 4048-4050 (2004)

[24] S. M. Gruner, M. W. Tate, E. F. Eikenberry, *Rev. Sci. Instrum.* **73**, 2815-2842 (2002)

[25] J. Howe, D. M. Chambers, C. Courtois, E. Förster, C. D. Gregory, I. M. Hall, O. Renner, I. Uschmann, N. C. Woolsey, *Rev. Sci. Instrum.* **77**, 036105 (2006)

[26] G. W. Fraser, A. F. Abbey, A. D. Holland, K. J. McCarthy, A. Owens, A. Wells, *Nucl. Instrum. Meth. A* **350**, 368-378 (1994)

[27] L. Strüder, *Nucl. Instrum. Meth. A* **454**, 73-113 (2000)

[28] T. M. V. Bootsma, E. J. van Zwet, A. G. Brinkman, J. W. den Herder, L. de Jong, P. de Korte, S. M. Olsthoorn, *Nucl. Instrum. Meth. A* **439**, 575-581 (2000)

[29] B. E. Burke, J. A. Gregory, A. M. Loomis, M. Lesser, M. W. Bautz, S. E. Kissel, D. D. Rathman, R. M. Osgood, M. J. Cooper, T. A. Lind, G. R. Ricker, *IEEE Trans. Nucl. Science* **51**, 2322-2327 (2004)

[30] R. E. Griffiths, G. Polucci, A. Mak, S. S. Murray, D. A. Schwartz, *Single photon X-ray imaging with charge-coupled devices*, SPIE proceedings **290**, 62-68 (1981)

[31] R. E. Griffiths, G. Polucci, A. Mak, S. S. Murray, D. A. Schwartz, M. V. Zombeck, *Preliminary results from a single-photon imaging X-ray charge-coupled device CCD camera*, SPIE proceedings **244**, 57-65 (1981)

[32] B. Mikulec, M. Campbell, E. Heijne, X. Llopart, L. Tlustos, *Nucl. Instrum. Meth. A* **511**, 282-286 (2003)

[33] T. E. Gureyev, S. Mayo, S. W. Wilkins, D. Paganin, A. W. Stevenson, *Phys. Rev. Lett.* **86**, 5827-5830 (2001)

[34] E. Takács, B. Radics, C. Szabó, S. Biri, L. T. Hudson, J. Imrek, B. Juhasz, T. Suta, A. Valek, J. Palinkas, *Nucl. Instrum. Meth. B* **235**, 120-125 (2005)

[35] S. Biri, A. Valek, T. Suta, E. Takács, Cs. Szabó, L. T. Hudson, B. Radics, J. Imrek, B. Juhász, J. Pálinkás, *Rev. Sci. Instrum.* **75**, 1420-1422 (2004)

[36] F. Zamponi, T. Kämpfer, A. Morak, I. Uschmann, E. Förster, *Rev. Sci. Instrum.* **76**, 116101 (2005)

[37] G. W. Fraser, X-ray detectors in astronmy, Cambridge University Press (Cambridge, 1989)

[38] M. W. Bautz, G. Y. Prigozhin, M. J. Pivovaroff, S. E. Jones, S. E. Kissel, G. R. Ricker, *Nucl. Instrum. Meth. A* **436**, 40-52 (1999)

[39] G. R. Hopkinson, *Nucl. Instrum. Meth. A* **216**, 423-429 (1983)

[40] G. Prigozhin, N. R. Butler, S. E. Kissel, G. R. Ricker, *IEEE Trans. Electr. Dev.* **50**, 246-253 (2003)

[41] G. G. Pavlov, J. A. Nousek, *Nucl. Instru. Meth. A* **428**, 348-366 (1999)
[42] L. Labate, M. Galimberti, A. Giulietti, D. Giulietti, L. A. Gizzi, P. Tomassini, G. Di Cocco, *Nucl. Instrum. Meth. A*, **495**, 148-153 (2002)
[43] D. Batani, *Laser Part. Beams*, **20**, 321-336 (2002)

Element	Kα (keV)	Kβ (keV)
Cr	5.41	5.95
Ni	7.48	8.26
Fe	6.40	7.06

TABLE I: Kα and Kβ line energy for the elements in the target relative to the spectrum of Figure (figure5).

Figure captions

Figure 1. Layout of the experimental setup.

Figure 2. Typical raw image as provided by our detectors. Such an image is obtained from one laser shot.

Figure 3. Pulse height distribution obtained from 350 laser shots irradiation of a Ti-Cu target, for the front side diagnostics shown in Figure (figure1).

Figure 4. *left:* Image of the X-ray source at the Ti Kα and Kβ energy (that is, considering together photons at both the Kα and Kβ energy of Ti) as seen from the front side of the target. The image refers to the same set of shots of Figure (figure3) (350 shots on a Ti-mylar-Cu target). The image size is 200 μm (in the object plane) in both the horizontal and vertical direction. *right:* Same as at left, but after the correction for the target position changes from shot to shot.

Figure 5. X-ray spectrum obtained from 350 laser shots irradiation of a Cr-Ni-Fe target.

Figure 6. X-ray images of the source at the Kα and Kβ energy (considered together) of the different target materials, obtained from 350 shots on a Cr-Ni-Fe target: *top:* Cr, *middle:* Ni, *bottom:* Fe. The image size is 156 μm (in the object plane) in both the horizontal and vertical direction.

Figure 7. Lineout along the horizontal direction, integrated over 10 μm in the vertical direction, of the top images of Figure (figure6).